analytical chemistry

Article

Cite This: Anal. Chem. 2018, 90, 12270−12277

pubs.acs.org/ac

SnS_2 Quantum Dots as New Emitters with Strong Electrochemiluminescence for Ultrasensitive Antibody Detection

Yan-Mei Lei, Jia Zhou, Ya-Qin Chai, Ying Zhuo,* and Ruo Yuan*

Key Laboratory of Luminescent and Real-Time Analytical Chemistry, Ministry of Education, College of Chemistry and Chemical Engineering, Southwest University, Chongqing 400715, China

Supporting Information

ABSTRACT: Herein, we designed an electrochemiluminescence (ECL) biosensor with SnS_2 quantum dots (SnS_2 QDs) as novel emitters for the ultrasensitive assay of cytomegalovirus pp65 antibody (anti-CMV pp65) via smart circular peptide-DNA nanomachine amplification. First, the novel ECL biosensing platform was constructed by self-assembly of water-soluble, nontoxic, and earth-abundant SnS_2 QDs on the 3D hierarchical silver nanoflowers (Ag NFs) surface, where the Ag NFs, as coreaction accelerator in the ECL ternary (SnS_2 QDs/$S_2O_8^{2-}$/Ag NFs) system, could efficiently boost the ECL intensity of SnS_2 QDs. Furthermore, we designed a specific nucleic acid sequence labeled antigenic peptide to act as multifunctionalized capture probe (CP), which could specifically recognize the target antibody assisting with two auxiliary DNA strands via the proximity hybridization of DNA motifs to form a smart circular peptide-DNA nanomachine. Then, with the aid of nuclease, the resultant circular peptide-DNA nanomachine could initiate the subsequent cascade recycling amplification to output massive DNA products as mimic target (MT). As a result, the proposed ECL biosensor for anti-CMV pp65 detection exhibited high sensitivity with a wide linear range from 1 fM to 100 nM and a low detection limit (0.33 fM). Importantly, this work not only first utilized SnS_2 QDs as promising ECL emitters for biosensing platform construction but also opened an efficient way for highly sensitive and selective detection of antibody in disease diagnosis and clinical analysis.

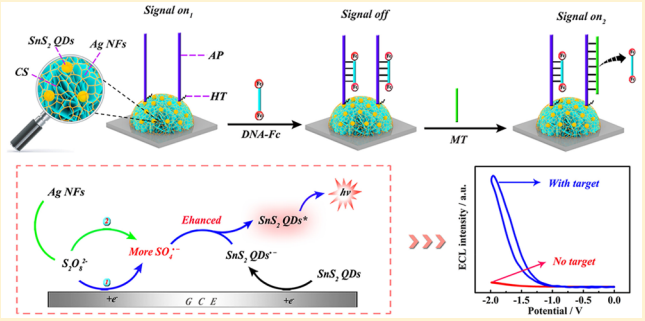

Colloidal semiconductor nanocrystals or quantum dots (QDs), as a new class of electrochemiluminescence (ECL) emitters, have recently stimulated keen interest owing to their unique characteristics of size- and shape-tunable luminescence, high quantum yield, and excellent photostability.[1−3] Until now, tremendous efforts have been made in the synthesis of different highly luminescent QDs, such as CdTe QDs, PbS QDs, and $CsPbI_3$ QDs.[4−6] Despite their exclusive popularity, the application of these QDs in biosensing fields is fundamentally restricted by the dependence on the highly toxic or rare elements. Therefore, the exploration of other new highly luminescent QDs constituted of nontoxic and environmentally benign elements is a challenging and interesting issue.[7,8] Recently, our group used the nontoxic MoS_2 QDs as ECL emitters to construct a practical and label-free aptasensor for the detection of lipopolysaccharide.[9] However, these MoS_2 QDs, obtained by chemical exfoliation from the bulk MoS_2 ("top-down" approach), are usually sensitive to the environment and needed for the harsh pretreatment procedures, resulting in the uncontrollable and unreproducible ECL response in different batches. Consequently, there is an urgent need to look for other new QDs with excellent ECL signal, which have more promising applications in the ECL bioanalysis. Tin disulfide (SnS_2), as a fullerene-like n-type semiconductor, has currently attracted much attention as low-cost, earth-abundant, and environmentally benign material for photodetectors, gas-sensoring, and lithium batteries.[10−12] However, as far as we know, there have been no reports on the ECL behavior of SnS_2 nanomaterials. Herein, water-soluble and colloidally robust SnS_2 QDs were synthesized by a facile and green L-cysteine-assisted hydrothermal method ("down-top" approach), which could be used as promising ECL emitters in peroxydisulfate ($S_2O_8^{2-}$) solution. Usually, the high concentration of $S_2O_8^{2-}$ solution (~100 mM) is an essential prerequisite to obtain a strong ECL response of QDs. However, it will inevitably inflict damage on the biosensing interface due to its strong oxidizing effect.[13] In this work, we utilized 3D hierarchical silver nanoflowers (Ag NFs) as coreaction accelerator to develop a novel ternary (SnS_2 QDs/$S_2O_8^{2-}$/Ag NFs) system, where the ECL intensity of SnS_2 QDs could be efficiently boosted at low $S_2O_8^{2-}$ concentration (~5 mM), achieving a nice analytical performance of biosensor.

It is well acknowledged that antibodies are important biomarkers for a range of diseases, including infectious diseases, autoimmune diseases, and allergies.[14,15] Thus, the highly sensitive and selective detection of antibody for early diagnosis and severity prediction in time will have important significance in preventing disease transmission and improving therapeutic

Received: August 10, 2018
Accepted: September 18, 2018
Published: September 18, 2018

DOI: 10.1021/acs.analchem.8b03623
Anal. Chem. 2018, 90, 12270−12277

Scheme 1. Schematic Illustration of the Prepared ECL Biosensor Toward Ultrasensitive Detection of Target Anti-CMV pp65[a]

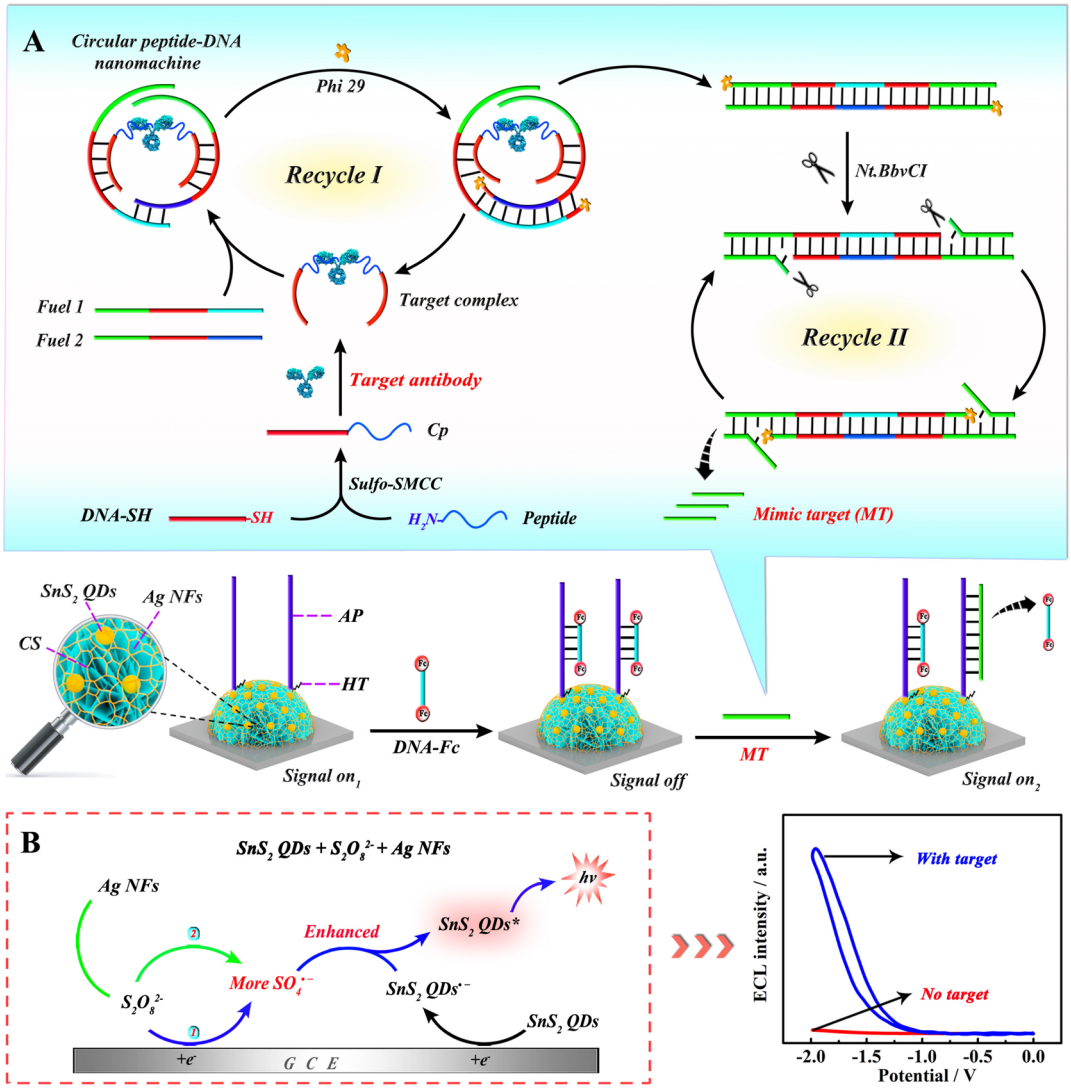

[a](A) Target-initiated circular peptide-DNA nanomachine cascade recycling amplification and (B) the possible ECL mechanism of the SnS_2 QDs/$S_2O_8^{2-}$/AgNFs system.

effects.[16] Recently, many DNA amplification strategies have been developed for the determination of nucleic acid, small molecule, protein, and metal ion with excellent sensitivity in biosensing fields.[17−20] Of particular note, the peptide-functionalized DNA strand to translate an antibody into a unique DNA strand is a promising and highly efficient approach owing to its unique advantages, such as cost effectiveness, excellent specific, and strong affinity.[21,22] For example, Ranallo and co-workers recently constructed a modular DNA-nanomachine capable of loading/releasing a DNA cargo in the presence of a specific antibody.[23] Merkx's group also utilized the characteristic bivalent architecture of antibody to accelerate DNA-strand exchange reaction.[24] These strategies only transferred the target antibody into DNA strand, but the lack of the target recycling induced signal amplification could limit the further improvement of the analysis performance. In response to this, here, we designed a specific nucleic acid sequence labeled antigenic peptide, as a multifunctionalized capture probe (CP), which could specifically recognize the target antibody assisting with two auxiliary DNA strands via the proximity hybridization of DNA motifs to form a smart circular peptide-DNA nanomachine. Then, with the aid of nuclease, the resultant circular peptide-DNA nanomachine could initiate the subsequent cascade recycling amplification to output massive DNA products as mimic target (MT).

Human cytomegalovirus (CMV) infection is the most frequent cause of congenital infections, which associate with a variety of pathological conditions, such as retinitis, encephalitis, hepatitis, and pneumonia that may be transmitted congenitally, horizontally, and parenterally and occurs both as a primary infection and as reactivation in immunocompromised individuals.[25] In this work, an ECL biosensor with SnS_2 QDs as novel emitters was designed for highly sensitive detection of cytomegalovirus pp65 antibody (anti-CMV pp65) via smart circular peptide-DNA nanomachine amplification. As depicted in Scheme 1, the 3D hierarchical silver nanoflowers (Ag NFs) were obtained by a simple electrochemical deposition method, which could not only act as a substrate material possessing large specific surface area for the immobilization of massive SnS_2 QDs but also act as a new coreaction accelerator toward the ECL ternary (SnS_2 QDs/$S_2O_8^{2-}$/Ag NFs) system for remarkably enhanced ECL signal. Then, chitosan (CS) solution was modified onto the SnS_2 QDs surface for further cross-linking

DOI: 10.1021/acs.analchem.8b03623
Anal. Chem. 2018, 90, 12270−12277

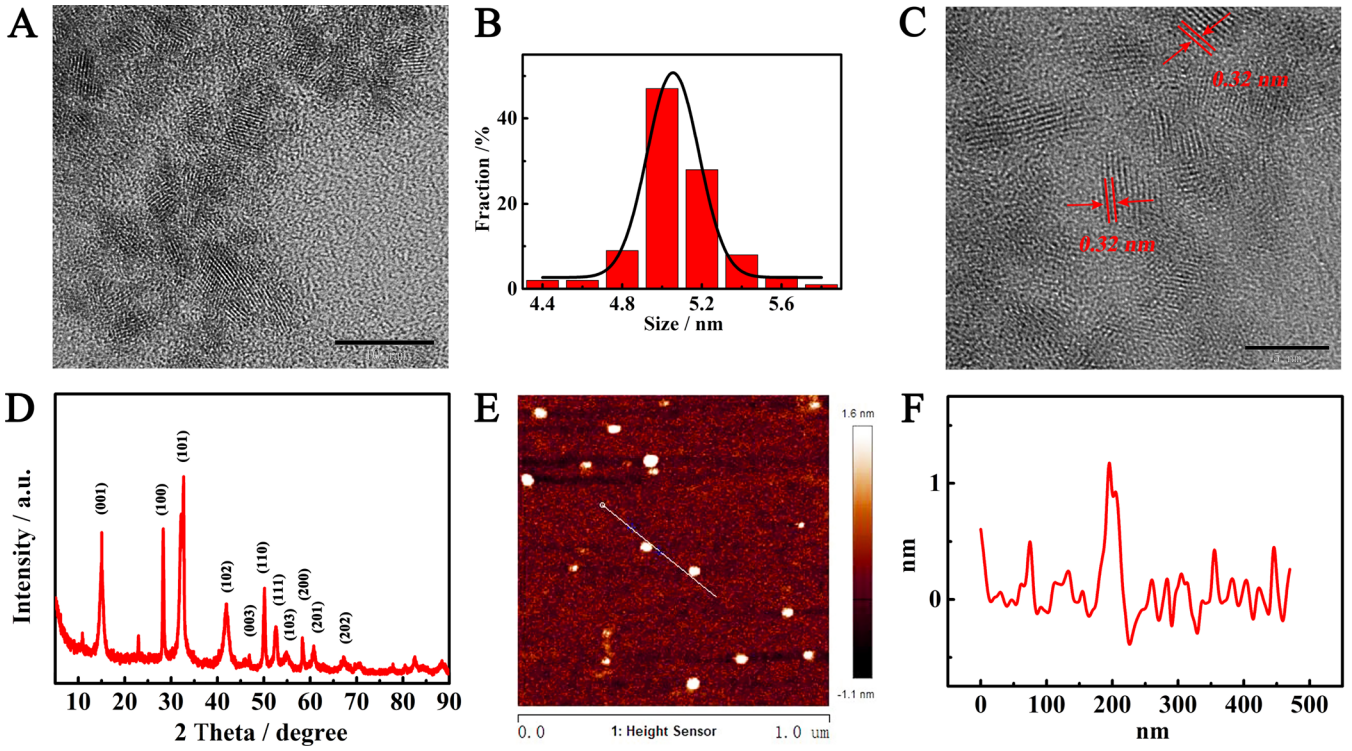

Figure 1. (A) HR-TEM image (scale bar, 10 nm), (B) the diameter distribution, and (C) HR-TEM image (scale bar, 5 nm) of the SnS_2 QDs. (D) XRD analysis of the SnS_2 QDs. (E) AFM image and (F) height profile of the SnS_2 QDs.

with the amino-modified assistant probe (AP), achieving a strong ECL initial signal (which acted as "signal on$_1$" state) in $S_2O_8^{2-}$ solution. Subsequently, the quencher probes of Fc modified DNA strands (DNA-Fc) were hybridized with the AP, resulting in an extremely low ECL signal to obtain the "signal off" state. In the presence of anti-CMV pp65, the designed multifunctionalized CP could specifically recognize the antibody with the aid of two auxiliary DNA strands via the proximity hybridization of DNA motifs to form a smart circular peptide-DNA nanomachine, which could further initiate the subsequent cascade recycling amplification with help of nuclease to output massive MT products. Finally, the MT products were captured by the AP to make DNA-Fc be released from the electrode surface; the ECL intensity was recovered to get the "signal on$_2$" state. As expected, the prepared ECL biosensing platform achieved high sensitivity for the anti-CMV pp65 assay. Significantly, this work not only exhibited the SnS_2 QDs as promising ECL emitters for biosensing platform construction but also opened a new way for highly sensitive and selective detection of antibody in disease diagnosis and clinical analysis.

EXPERIMENTAL SECTION

Preparation of the SnS_2 QDs. SnS_2 QDs were synthesized through a one-pot and green hydrothermal method according to a modified literature procedure.[26] First, 6.0 mM $SnCl_4 \cdot 5H_2O$ and 20 mM L-cysteine as a sulfur source were dissolved in 25 mL of ultrapure water to form a transparent precursor solution. Thereafter, the above mixture was heated in a 50 mL Teflon-lined stainless-steel autoclave at 180 °C for 6 h. The yellow supernatant was collected by centrifugation (12 000 rpm, 15 min at 4 °C) to remove the residue of reactants, which was further dialyzed in a dialysis bag (retained molecular weight: 3000 Da) to obtain SnS_2 QDs.

Preparation of the Multifunctionalized Capture Probe. The multifunctionalized capture probe (CP) was obtained according to the literature with slight modifications.[23] First, the CMV pp65 peptide was dissolved in PBS (pH 7.4) solution and mixed with 20-fold excess of sulfosuccinimidyl 4-(*N*-maleimidomethyl)cyclohexane-1-carboxylate (Sulfo-SMCC) in 50% dimethylformamide for 2 h at room temperature, followed by removal of nonreacted reagent by dialysis. Subsequently, the Sulfo-SMCC-CMV pp65 peptide was dissolved in 100 mM sodium phosphate (pH 7.0) solution and mixed with a 10-fold excess of tris(2-carboxyethyl) phosphine hydrochloride (TCEP)-activated thiol-modified DNA (DNA-SH) for 2 h. Finally, the obtained oligonucleotide−peptide conjugate as capture probe (CP) was stored at 4 °C for further use.

Preparation of the ECL Biosensor. First, the cleaned glassy carbon electrode (GCE, Φ = 4.0 mm) was immersed in 2 mL of electrolyte solution (containing 5 mM $AgNO_3$, 0.2 M KNO_3, 1 mM sodium citrate dihydrate, and 2.5 g/L polyvinylpyrrolidone) to obtain the 3D hierarchical Ag NFs by electrochemical deposition under a constant potential at 0.25 V for 30 min. Then, 5 μL of the prepared SnS_2 QDs solution was dropped onto the above modified electrode to immobilize SnS_2 QDs on the Ag NFs surface via Ag−S bonds. Following that, 5 μL of CS solution (0.02%) was dropped onto the resultant electrode (GCE/Ag NFs/SnS_2 QDs) and dried at room temperature. Then, 10 μL of AP solution (0.5 μM) with carboxy-group was modified on the resultant electrode (GCE/Ag NFs/SnS_2 QDs/CS) surface via EDC/NHS cross-linking at 4 °C for 5 h. Next, the resultant electrode (GCE/Ag NFs/SnS_2 QDs/CS/AP) was incubated with HT (15 μL, 1 mM) for 40 min. Finally, 10 μL of Fc modified DNA strand (DNA-Fc, 2 μM) was further incubated on the above modified electrode for 2 h; the biosensor (GCE/Ag NFs/SnS_2 QDs/CS/AP/HT/DNA-Fc) was achieved and stored at 4 °C for further use.

DOI: 10.1021/acs.analchem.8b03623
Anal. Chem. 2018, 90, 12270−12277

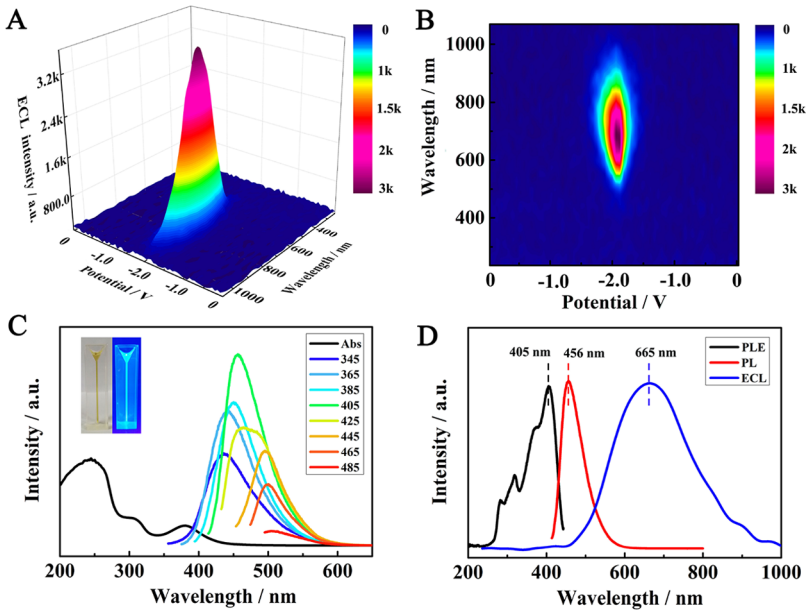

Figure 2. (A) 3D surface image model and (B) heat map image of the prepared SnS_2 QDs in 5.0 mM $S_2O_8^{2-}$ solution. (C) UV−vis absorption and PL spectrum of the prepared SnS_2 QDs aqueous suspension at different excitation wavelengths. The inset of C was the photographs of the prepared SnS_2 QDs aqueous suspension under visible light (left) and UV irradiation (right) light. (D) PL excitation (PLE) spectrum, PL spectrum, and maximum ECL spectrum (with potential at −2.0 V) of the prepared SnS_2 QDs aqueous suspension.

Target-Initiated Circular Peptide-DNA Nanomachine Cascade Recycling Amplification. Target-initiated circular peptide-DNA nanomachine cascade recycling amplification was carried out by the following steps: First, 5 μL of anti-CMV pp65 solution with different concentrations was mixed with 1 μL of CP (1 μM) to produce "target complex". Then, the "target complex" reacted with 5 μL of Fuel strands (5 μM Fuel 1 and 5 μM Fuel 2) to form a circular peptide-DNA nanomachine. Next, the above reaction solution was mixed with 20 μL of substrate solution containing 500 μM dNTPs, 100 U/mL phi29 DNA polymerase, and 100 U/mL Nt.BbvCI and incubated with the mixture at 37 °C for 2 h. Remarkably, the target-initiated circular peptide-DNA nanomachine cascade recycling amplification included two processes. In recycle I, the circular peptide-DNA nanomachine was activated by phi29 DNA polymerase to generate the double-stranded DNA (ds DNA) template and target complex, where the target complex could in turn trigger the recycle I with the aid of Fuel 1 and Fuel 2 to release more ds DNA template. Meanwhile, in the presence of Nt.BbvCI, the ds DNA template could further initiate the subsequent strand displacement amplification to output massive MT products. Finally, the replication procedure was suppressed by a thermal treatment at 85 °C for 10 min, and the resultant MT solution was used for the following measurement process.

Measurement Procedure. The measurement procedure was carried out as follows: First, 10 μL of MT solution was incubated on the proposed ECL biosensor for 2 h, which then was rinsed with ultrapure water to remove the redundant MT. Following that, the ECL response was investigated with a MPI-E multifunctional electrochemical and chemiluminescent analytical system in 3.0 mL of $K_2S_2O_8$ (5 mM, pH 7.4) solution, where the scan potential was varied from −2.0 to 0 V and the voltage of the photomultiplier tube (PMT) was set at 800 V.

RESULTS AND DISCUSSION

Physicochemical Characterization of the Prepared SnS_2 QDs. The typical high-resolution TEM (HR-TEM) images in Figure 1A showed the prepared SnS_2 QDs exhibited monodisperse crystalline with a uniform lateral diameter around 5.0 nm (Figure 1B). As expected, the HR-TEM images in Figure 1C showed the lattice constant of SnS_2 QDs is 0.32 nm, which corresponded to the 6-fold symmetry of (100) plane of hexagonal crystal SnS_2.[27] Energy dispersive X-ray (EDX) analysis (as shown in the Figure S2) showed Sn, S, C, and O signals, confirming the SnS_2 stoichiometry with a Sn/S ratio of 66.35:36.65.[28] In addition, X-ray diffraction (XRD) was performed for further phase confirmation. From Figure 1D, the primary diffraction peaks of the as-prepared SnS_2 QDs matched with the hexagonal 2H SnS_2 structure (space group = $P\bar{3}m1$, ICDD 23-0677), which extended over only one monolayer. Meanwhile, the small diffraction peaks at ∼58 and ∼50 suggested the coexistence of 4H SnS_2 structure (space group = *P63mc*, ICDD 21-1231), which extended over two monolayers.[29] The thickness of the as-prepared SnS_2 QDs was also analyzed by atomic force microscopy (AFM) topography images. A white line profile painted on the AFM image (Figure 1F) exhibited that the thickness is less than 1.2 nm (Figure 1E), corresponding well with that of 1−2 layers of SnS_2 QDs.[30]

The 3D surface image model (Figure 2A) and heat map image (Figure 2B) of the prepared SnS_2 QDs with $S_2O_8^{2-}$ as coreactant showed the maximum ECL emission at 665 nm with potential at −2.0 V. Further UV−vis absorption and photoluminescence (PL) spectrum analysis of SnS_2 QDs were shown in Figure 2C. The UV−vis absorption spectrum (black line) was observed with three characteristic absorption bands at 245 nm (5.06 eV), 305 nm (4.07 eV), and 380 nm (3.26 eV). The absorption at 305 nm (4.06 eV) and 380 nm (3.26 eV) might be related to the indirect excitonic transition from the Γ to the M point of the Brillouin zone in 2H and 4H SnS_2 structures,[29] while the adsorption at 245 nm (5.06 eV) should result from the direct excitonic transition at the M point for both 2H and 4H structures.[31] Furthermore, the PL spectrum of SnS_2 QDs exhibited an excitation-dependent PL phenomenon

DOI: 10.1021/acs.analchem.8b03623
Anal. Chem. 2018, 90, 12270−12277

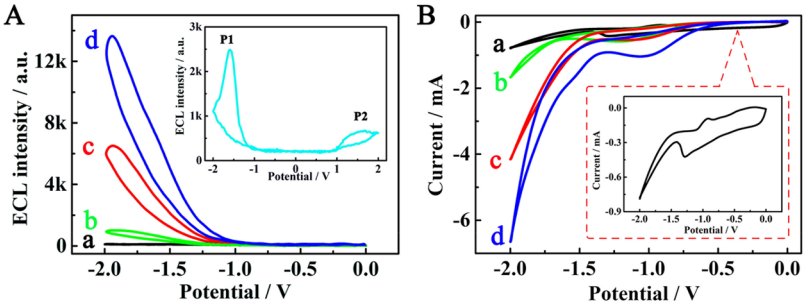

Figure 3. Synchronous (A) ECL and (B) CV curves of the different systems: bare GCE in (a) SnS_2 QDs + PBS + Na_2SO_3, (b) $S_2O_8^{2-}$, and (c) SnS_2 QDs + $S_2O_8^{2-}$ and (d) Ag NFs/GCE in SnS_2 QDs + $S_2O_8^{2-}$. The inset of (A) is the ECL curve of bare GCE in SnS_2 QDs + PBS + Na_2SO_3 (scan range: −2.0 to 2.0 V, vs Ag/AgCl). The inset of (B) is the amplification of curves a. The concentrations of SnS_2 QDs, $S_2O_8^{2-}$, and Na_2SO_3 were 0.1 mg/mL, 5.0 mM, and 1 mM in PBS (pH 7.4), respectively.

(Figure 2C). When the excitation wavelength was varied from 345 to 485 nm, the PL peak moved to the longer wavelengths and its intensity decreased obviously owing to quantum size effect.[32] Correspondingly, it emitted the maximum emission wavelength at 456 nm with an excitation wavelength of 405 nm. In addition, the SnS_2 QDs exhibited a light yellow color under visible light and emitted blue fluorescence by irradiating at 365 nm with a UV lamp (the inset of Figure 2C). Figure 2D showed the maximum ECL spectrum of SnS_2 QDs (blue line) with emission peak at 665 nm, which had an obvious 209 nm red-shift compared with the PL spectrum of SnS_2 QDs owing to the contribution of the vacancy defect.[33]

Possible ECL Mechanism of the Prepared SnS_2 QDs. To clarify the ECL reaction mechanism of the SnS_2 QDs, as shown in Figure 3, ECL and CV measurements were synchronously implemented during a potential scan cycle between −2.0 and 0 V. Almost no ECL signal was observed (Figure 3A, curve a) when bare GCE was detected in the SnS_2 QDs + PBS + Na_2SO_3 system (where Na_2SO_3 was used to remove dissolved oxygen),[33] and the corresponding CV curve exhibited an evident reduction peak at −1.25 V (Figure 3B, curve a), indicating that the negatively charged SnS_2 QDs (SnS_2 QDs$^{\bullet-}$) were produced by injecting electrons into the unoccupied molecular orbitals (LUMOs).[3] Remarkably, when bare GCE was detected in the above system with the wider potential from −2.0 to 2.0 V, two evident ECL peaks of high cathodic peak (P1, about 2439 a.u.) and low anodic peak (P2, about 625 a.u.) were observed (the inset of Figure 3A). This was because the positively charged SnS_2 QDs (SnS_2 QDs$^{\bullet+}$) were generated by injecting holes onto the highest occupied molecular orbitals (HOMOs) at positive scanning, which could collide with the more stable SnS_2 QDs$^{\bullet-}$ to produce the excited state of SnS_2 QDs (SnS_2 QDs*) and emitted light. Subsequently, when bare GCE was detected in $S_2O_8^{2-}$ solution, a slightly obvious ECL intensity of about 1000 a.u. was obtained (Figure 3A, curve b), corresponding to the emission of the singlet oxygen ($^1(O_2)_2$*).[34] The corresponding CV curve displayed an appreciable reduction peak at −1.20 V (Figure 3B, curve b), which indicated that the strong oxidizing intermediates (sulfate radical anion, $SO_4^{\bullet-}$) were generated by the electrochemical reduction process.[35] Significantly, when bare GCE was detected in the SnS_2 QDs + $S_2O_8^{2-}$ system, the ECL intensity of ∼6458 a.u. was obviously increased by 6.5 times (Figure 3A, curve c) in comparison to that of $S_2O_8^{2-}$ solution (Figure 3A, curve b). This was attributed to fact that the generation of SnS_2 QDs$^{\bullet-}$ could react with $SO_4^{\bullet-}$ to produce the more excited state of SnS_2 QDs (SnS_2 QDs*) and emitted strong light. The corresponding CV wave (Figure 3B, curve c) exhibited the more positive reduction potential at−1.10 V and the higher peak current, demonstrating the strong interaction between SnS_2 QDs and $S_2O_8^{2-}$. More interestingly, when Ag NFs/GCE modified electrode was detected in the SnS_2 QDs + $S_2O_8^{2-}$ system, the ECL intensity of ∼13 731 a.u. was obviously increased (Figure 3A, curve d) by 13.7 times in comparison to that of curve b in Figure 3A, demonstrating that the Ag NFs acted as an efficient coreaction accelerator to speed up the reduction of $S_2O_8^{2-}$ to produce more $SO_4^{\bullet-}$ and thus achieving a strong emission of SnS_2 QDs*. The corresponding CV curve exhibited the more positive reduction potential at −1.05 V and the higher peak current (Figure 3B, curve d) in comparison to that of curve c in Figure 3B, demonstrating that the Ag NFs could speed up the interaction between SnS_2 QDs and $S_2O_8^{2-}$. Herein, we could presume that the generated Ag(I) ions on the surface of Ag NFs via the electrochemical reaction could actually speed up the reduction of $S_2O_8^{2-}$ to output massive $SO_4^{\bullet-}$, which could further react with SnS_2 QDs to produce more SnS_2 QDs*, achieving a very strong ECL intensity.[36] Consequently, the ECL reaction mechanism of the SnS_2 QDs could be summarized in the following eqs 1−4.

$$SnS_2QDs + e^- \rightarrow SnS_2QDs^{-\bullet} \quad (1)$$

$$S_2O_8^{2-} + e^- \xrightarrow{AgNFs} SO_4^{-\bullet} \quad (2)$$

$$SO_4^{-\bullet} + SnS_2QDs^{-\bullet} \rightarrow SnS_2QDs^* + SO_4^{2-} \quad (3)$$

$$SnS_2QDs^* \rightarrow SnS_2QDs + h\nu \quad (4)$$

Optimization of the Experimental Conditions. To achieve the optimal assay performance, as shown in Figure 4, effects of the DNA-Fc concentration and the CP and DNA-Fc incubation time (in the presence of target) on the ECL signal of the as-proposed biosensor were investigated. According to Figure 4A, the ECL intensity decreased accordingly along with increasing DNA-Fc concentration from 0.5 to 3.0 μM and reached a maximum value at 2 μM. Thus, the concentration of DNA-Fc was fixed at 2 μM for the subsequent experiments. Figure 4B showed that the ECL signal increased accordingly with extending incubation time from 0.5 to 3.0 h and reached a plateau at 2 h. Therefore, the optimum incubation time of the CP and DNA-Fc was chosen as 2 h.

ECL Analysis of the Proposed Biosensor for Anti-CMV pp65 Detection. To evaluate the sensitivity of the proposed ECL biosensor, the quantitative measurement was performed by detecting different concentrations of anti-CMV pp65 under

DOI: 10.1021/acs.analchem.8b03623
Anal. Chem. 2018, 90, 12270−12277

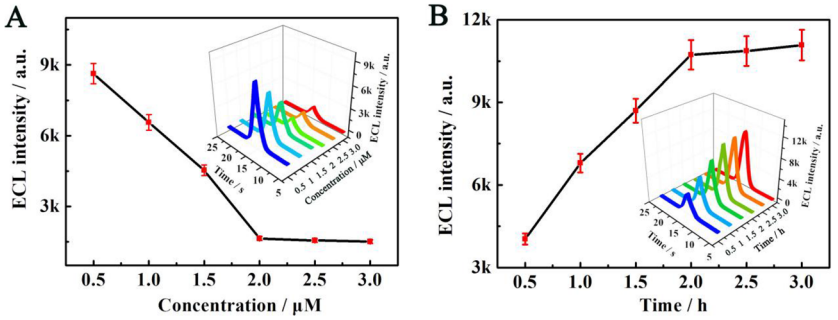

Figure 4. Effects of (A) the immobilization concentration of DNA-Fc and (B) the incubation time of CP and DNA-Fc (in the presence of target antibody) on the ECL intensity of the proposed biosensor. Error bars were the standard deviations of three parallel experiments.

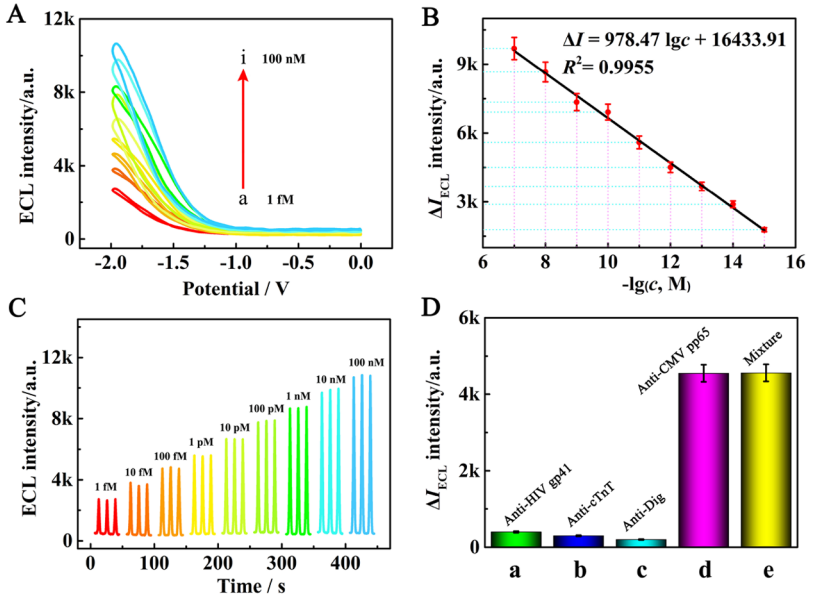

Figure 5. (A) ECL response of the proposed biosensors with different concentrations of anti-CMV pp65. (B) Calibration plot of the ΔI_{ECL} intensity vs. the logarithm of anti-CMV pp65 concentration. (C) Stability of the proposed biosensors in various concentrations of anti-CMV pp65. (D) Selectivity of the proposed biosensors against different targets: (a) anti-HIV gp41 (100 pM), (b) anti-cTnT (100 pM), (c) anti-Dig (100 pM), (d) anti-CMV pp65 (1 pM), and (e) a mixture containing 100 pM anti-HIV gp41, 100 pM anti-cTnT, 100 pM anti-Dig, and 1 pM anti-CMV pp65.

the optimal reaction conditions. As shown in Figure 5A from curve a to curve i, the ECL intensity increased accordingly with increasing anti-CMV pp65 concentrations (from 1 fM to 100 nM). The linear relationship between the changes in ECL intensities (ΔI_{ECL}) and the logarithmic values of anti-CMV pp65 concentration (lg c) was plotted in Figure 5B, fitted as ΔI_{ECL} = 978.47 lg c + 16433.91, and the detection limit was estimated at 0.33 fM (S/N = 3). In addition, the performance comparison among various test platforms was listed in Table S2, indicating that the proposed biosensor exhibited the highest sensitivity for antibody detection due to the smart circular peptide-DNA nanomachine amplification employed.

The stability of the proposed biosensor was investigated with different concentrations of anti-CMV pp65. As shown in Figure 5C, with the increase of anti-CMV pp 65 concentration (from 1 fM to 100 nM), the ECL intensity increased correspondingly and stable ECL curves were achieved under continuous CV scanning for 3 cycles, which indicated that the proposed biosensor had excellent stability for detection of anti-CMV pp65.

To further investigate the selectivity of the proposed biosensor for anti-CMV pp65 detection, the proposed biosensor was tested with different interference agents, including anti-CMV pp65, antihuman immunodeficiency virus gp41 (anti-HIV gp41), anticardiac troponin T (anti-cTnT), and antidigoxigenin (anti-Dig). As shown in Figure 5D, the interference agents exhibited negligible interference with anti-CMV pp65 selectivity, which suggested that the proposed biosensor had an excellent selectivity for the detection of anti-CMV pp65 over interference agents.

Detection of Anti-CMV pp65 in Real Samples. To investigate the clinical application potential of the prepared biosensor, recovery experiments were performed for anti-CMV pp65 detection in human serum by the standard addition method. The anti-CMV pp65 with different concentrations (defined as added) was added in 50% human serum (diluted by PBS solution), which was measured (defined as found) by using the prepared biosensor. The recovery was the ratio between the found and added, which was closely related to the accuracy of the prepared biosensor. As shown in Table 1, the recoveries were between 97.78% and 108.20%, demonstrating the good potential application of the prepared biosensor in disease diagnosis and clinical analysis.

CONCLUSIONS

In summary, an ECL biosensor with SnS_2 QDs as novel emitters was successfully developed for the ultrasensitive assay

DOI: 10.1021/acs.analchem.8b03623
Anal. Chem. 2018, 90, 12270−12277

Table 1. Determination of Anti-CMV pp65 in Normal Human Serum with the Proposed Method

sample number	added/pM	found/pM	recovery/%
1	1.00	1.04	104.00
2	10.00	10.82	108.20
3	20.00	19.89	99.45
4	50.00	50.01	100.02
5	100.00	97.78	97.78

of anti-CMV pp65 by coupling with the smart circular peptide-DNA nanomachine amplification. First, the novel ECL biosensing platform was obtained by self-assembly of SnS_2 QDs on the 3D hierarchical Ag NFs surface, where the coreaction accelerator of Ag NFs could efficiently enhance the ECL intensity of SnS_2 QDs at low $S_2O_8^{2-}$ concentration. Furthermore, the smart circular peptide-DNA nanomachine was first designed in this work to realize target recycling amplification, which could initiate the subsequent SDA to output massive MT products. Compared to the traditional antibody detection, the proposed ECL biosensor exhibited a high sensitivity and good selectivity for anti-CMV pp65 detection. Importantly, this work not only first investigated the ECL behavior of SnS_2 QDs and utilized SnS_2 QDs as ECL emitters for biosensing platform construction but also offered an efficient way for highly sensitive and selective detection of antibody in disease diagnosis and clinical analysis.

■ ASSOCIATED CONTENT

Supporting Information

The Supporting Information is available free of charge on the ACS Publications website at DOI: 10.1021/acs.analchem.8b03623.

Reagents and materials, apparatus, scanning electron microscopy characterization of 3D hierarchical Ag NFs, EDX analysis spectrum of the prepared SnS_2 QDs, characterization of the prepared ECL biosensor, and comparison of the other test platforms for antibody detection (PDF)

■ AUTHOR INFORMATION

Corresponding Authors

*Tel.: +86 23 68252277. Fax: +86 23 68253172. E-mail: yingzhuo@swu.edu.cn (Y.Z.).

*Tel.: +86 23 68252277. Fax: +86 23 68253172. E-mail: yuanruo@swu.edu.cn (R.Y.).

ORCID

Ya-Qin Chai: 0000-0003-4392-9592

Ying Zhuo: 0000-0002-4491-1186

Ruo Yuan: 0000-0003-3664-6236

Notes

The authors declare no competing financial interest.

■ ACKNOWLEDGMENTS

This work was financially supported by the National Natural Science Foundation of China (21775124, 21675130, and 21675129), the Natural Science Foundation Project of CQ CSTC (cstc2018jcyjAX0546), and the Fundamental Research Funds for the Central Universities, China (XDJK2018AA003).

■ REFERENCES

(1) Zebibula, A.; Alifu, N.; Xia, L.; Sun, C.; Yu, X.; Xue, D.; Liu, L.; Li, G.; Qian, J. *Adv. Funct. Mater.* **2018**, *28*, 1703451.

(2) Liu, H.; Wu, Z.; Shao, J.; Yao, D.; Gao, H.; Liu, Y.; Yu, W.; Zhang, H.; Yang, B. *ACS Nano* **2017**, *11*, 2239−2247.

(3) Tan, X.; Zhang, B.; Zou, G. *J. Am. Chem. Soc.* **2017**, *139*, 8772−8776.

(4) Yang, X.; Yu, Y. Q.; Peng, L. Z.; Lei, Y. M.; Chai, Y. Q.; Yuan, R.; Zhuo, Y. *Anal. Chem.* **2018**, *90*, 3995−4002.

(5) Dai, W. X.; Zhang, L.; Zhao, W. W.; Yu, X. D.; Xu, J. J.; Chen, H. Y. *Anal. Chem.* **2017**, *89*, 8070−8078.

(6) Imran, M.; Caligiuri, V.; Wang, M.; Goldoni, L.; Prato, M.; Krahne, R.; De Trizio, L.; Manna, L. *J. Am. Chem. Soc.* **2018**, *140*, 2656−2664.

(7) Xiong, M.; Rong, Q.; Meng, H. M.; Zhang, X. B. *Biosens. Bioelectron.* **2017**, *89*, 212−223.

(8) Feng, L. L.; Wu, Y. X.; Zhang, D. L.; Hu, X. X.; Zhang, J.; Wang, P.; Song, Z. L.; Zhang, X. B.; Tan, W. *Anal. Chem.* **2017**, *89*, 4077−4084.

(9) Zhao, M.; Chen, A. Y.; Huang, D.; Chai, Y. Q.; Zhuo, Y.; Yuan, R. *Anal. Chem.* **2017**, *89*, 8335−8342.

(10) Huang, Y.; Sutter, E.; Sadowski, J. T.; Cotlet, M.; Monti, O. L. A.; Racke, D. A.; Neupane, M. R.; Wickramaratne, D.; Lake, R. K.; Parkinson, B. A.; Sutter, P. *ACS Nano* **2014**, *8*, 10743−10755.

(11) Burton, L. A.; Whittles, T. J.; Hesp, D.; Linhart, W. M.; Skelton, J. M.; Hou, B.; Webster, R. F.; O'Dowd, G.; Reece, C.; Cherns, D.; Fermin, D. J.; Veal, T. D.; Dhanak, V. R.; Walsh, A. *J. Mater. Chem. A* **2016**, *4*, 1312−1318.

(12) Youn, D. H.; Stauffer, S. K.; Xiao, P.; Park, H.; Nam, Y.; Dolocan, A.; Henkelman, G.; Heller, A.; Mullins, C. B. *ACS Nano* **2016**, *10*, 10778−10788.

(13) Irkham; Watanabe, T.; Fiorani, A.; Valenti, G.; Paolucci, F.; Einaga, Y. *J. Am. Chem. Soc.* **2016**, *138*, 15636−15641.

(14) Golynskiy, M. V.; Rurup, W. F.; Merkx, M. *ChemBioChem* **2010**, *11*, 2264−2267.

(15) Banala, S.; Aper, S. J.; Schalk, W.; Merkx, M. *ACS Chem. Biol.* **2013**, *8*, 2127−2132.

(16) Banala, S.; Arts, R.; Aper, S. J.; Merkx, M. *Org. Biomol. Chem.* **2013**, *11*, 7642−7649.

(17) Zhao, X. H.; Gong, L.; Zhang, X. B.; Yang, B.; Fu, T.; Hu, R.; Tan, W. H.; Yu, R. Q. *Anal. Chem.* **2013**, *85*, 3614−3620.

(18) Lu, L. M.; Zhang, X. B.; Kong, R. M.; Yang, B.; Tan, W. *J. Am. Chem. Soc.* **2011**, *133*, 11686−11691.

(19) Zhang, X. B.; Wang, Z.; Xing, H.; Xiang, Y.; Lu, Y. *Anal. Chem.* **2010**, *82*, 5005−5011.

(20) Zhang, P.; Jiang, J.; Yuan, R.; Zhuo, Y.; Chai, Y. Q. *J. Am. Chem. Soc.* **2018**, *140*, 9361−9364.

(21) Wang, H. J.; Yuan, Y. L.; Chai, Y. Q.; Yuan, R. *Small* **2015**, *11*, 3703−3709.

(22) van Rosmalen, M.; Ni, Y.; Vervoort, D. F.; Arts, R.; Ludwig, S. K.; Merkx, M. *Anal. Chem.* **2018**, *90*, 3592−3599.

(23) Ranallo, S.; Prévost-Tremblay, C.; Idili, A.; Vallée-Bélisle, A.; Ricci, F. *Nat. Commun.* **2017**, *8*, 15150.

(24) Engelen, W.; Meijer, L. H. H.; Somers, B.; De Greef, T. F. A.; Merkx, M. *Nat. Commun.* **2017**, *8*, 14473−14481.

(25) Burbelo, P. D.; Issa, A. T.; Ching, K. H.; Exner, M.; Drew, W. L.; Alter, H. J.; Iadarola, M. J. *Virol. J.* **2009**, *6*, 45.

(26) Youn, D. H.; Stauffer, S. K.; Xiao, P.; Park, H.; Nam, Y.; Dolocan, A.; Henkelman, G.; Heller, A.; Mullins, C. B. *ACS Nano* **2016**, *10*, 10778−10788.

(27) Su, G.; Hadjiev, V. G.; Loya, P. E.; Zhang, J.; Lei, S.; Maharjan, S.; Dong, P.; Ajayan, P. M.; Lou, J.; Peng, H. *Nano Lett.* **2015**, *15*, 506−513.

(28) Shown, I.; Samireddi, S.; Chang, Y. C.; Putikam, R.; Chang, P. H.; Sabbah, A.; Fu, F. Y.; Chen, W. F.; Wu, C.; Yu, T. Y.; Chung, P. W.; Lin, M. C.; Chen, L. C.; Chen, K. H. *Nat. Commun.* **2018**, *9*, 169.

(29) Ou, J. Z.; Ge, W.; Carey, B.; Daeneke, T.; Rotbart, A.; Shan, W.; Wang, Y.; Fu, Z.; Chrimes, A. F.; Wlodarski, W.; Russo, S. P.; Li, Y. X.; Kalantar-zadeh, K. *ACS Nano* **2015**, *9*, 10313−10323.

(30) Huang, Y.; Sutter, E.; Sadowski, J. T.; Cotlet, M.; Monti, O. L. A.; Racke, D. A.; Neupane, M. R.; Wickramaratne, D.; Lake, R. K.; Parkinson, B. A.; Sutter, P. *ACS Nano* **2014**, *8*, 10743−10755.

DOI: 10.1021/acs.analchem.8b03623
Anal. Chem. 2018, 90, 12270−12277

(31) Seminovski, Y.; Palacios, P.; Wahnón, P. *Thin Solid Films* **2013**, *535*, 387−389.
(32) Du, Y.; Yin, Z.; Rui, X.; Zeng, Z.; Wu, X. J.; Liu, J.; Zhu, Y.; Zhu, J.; Huang, X.; Yan, Q.; Zhang, H. *Nanoscale* **2013**, *5*, 1456−1459.
(33) Wang, F.; Lin, J.; Zhao, T.; Hu, D.; Wu, T.; Liu, Y. *J. Am. Chem. Soc.* **2016**, *138*, 7718−7724.
(34) Lei, Y. M.; Zhao, M.; Wang, A.; Yu, Y. Q.; Chai, Y. Q.; Yuan, R.; Zhuo, Y. *Chem. - Eur. J.* **2016**, *22*, 8207−8214.
(35) Ma, M. N.; Zhuo, Y.; Yuan, R.; Chai, Y. Q. *Anal. Chem.* **2015**, *87*, 11389−11397.
(36) Lei, Y. M.; Wen, R. X.; Zhou, J.; Chai, Y. Q.; Yuan, R.; Zhuo, Y. *Anal. Chem.* **2018**, *90*, 6851−6858.

DOI: 10.1021/acs.analchem.8b03623
Anal. Chem. 2018, 90, 12270−12277